Data bank for interpreting results of polarization sensing of crystalline clouds

D.N. Romashov, B.V. Kaul', and I.V. Samokhvalov*

Institute of Atmospheric Optics,
Siberian Branch of the Russian Academy of Sciences, Tomsk
** Tomsk State University*

Received April 4, 2000

The structure of the backscattering phase matrix for hexagonal ice crystals is studied. The architecture and content of a data bank for interpreting the experimentally measured backscattering matrices of crystalline clouds are described. The beam splitting method is used for calculation of the data bank elements. Integral optical characteristics of the backscattering light are analyzed. Backscattering matrices of crystalline clouds obtained with the Stratosfera 1M lidar are compared with model matrices calculated with the use of the data bank. The close agreement between the model and measured matrices is demonstrated.

Introduction

This paper continues a series of works (Refs. 1–3) devoted to interpretation of the results of laser polarization sensing of crystalline clouds. At present there are many papers presenting both theoretical model studies and analysis of experimental results on the state of polarization of a backscattered and received lidar signal. Most of these papers are limited to measurement or calculation of the depolarization ratio $\delta = 2I_\perp/(I_\parallel + I_\perp)$ (Refs. 4 and 5) or measurement of only three Stokes parameters (I, Q, and U) of the backscattered signal (Ref. 6). Such an approach does not allow a comprehensive information on microstructure and orientation of ice crystals to be obtained. In Ref. 7 it was shown that the orientation of crystal axes with respect to the horizontal plane significantly affects the value of the extinction coefficient of the cirrus clouds. The most comprehensive information on the cirrus clouds microstructure can be obtained by analyzing the measured backscattering phase matrix (BSPM), provided that some *a priori* model calculated data on the scattering properties of ice crystals are available. This paper is devoted to solution of this problem. We restricted our consideration to the models of various hexagonal columns and plates. It should be noted that ice crystals of other shapes also fit into the proposed approach. Our further work will be devoted to accumulation and analysis of model calculated data on polarization properties of backscattering as applied to ice crystals of other shapes.

1. Structure of backscattering phase matrix of ensembles of poly-oriented hexagonal ice crystals

In Ref. 3 it was shown that BSPM elements $\mathbf{P}(a, L)$ for an ensemble of monodisperse hexagonal crystals oriented with the probability density of spatial orientation of crystal axes $g(\alpha, \beta)$ can be calculated by integrating over the full solid angle:

$$\mathbf{P}(a, L) = \frac{1}{4\pi} \int_0^{2\pi} \int_0^{\pi} \mathbf{M}(a, L, \alpha, \beta)\, g(\alpha, \beta) \sin\beta \, d\beta \, d\alpha; \tag{1}$$

$$\mathbf{M}(a, L, \alpha, \beta) = \mathbf{R}(-\alpha) \cdot \mathbf{M}(a, L, 0, \beta) \cdot \mathbf{R}(-\alpha),$$

where L is the length along the crystal axis; a is the radius of a circle circumscribed about the hexagonal base of the crystal; β is the angle between the direction of the incident radiation (axis Oz) and the crystal axis; α is the angle between the reference plane (xOz in Fig. 1) and the plane including the direction of incident radiation and the crystal axis; $\mathbf{M}(a, L, 0, \beta)$ is the BSPM averaged over the angle γ for hexagonal crystals whose axes lie in the reference plane ($\alpha = 0$) and make an angle β with the direction of incident radiation, γ is the angle of rotation about the crystal axis:

$$\mathbf{M}(a, L, 0, \beta) = \frac{3}{\pi} \int_0^{\pi/3} \mathbf{M}'(a, L, 0, \beta, \gamma)\, d\gamma,$$

where $\mathbf{M}'(a, L, 0, \beta, \gamma)$ is the BSPM of a crystal arbitrarily oriented in the reference plane; $\mathbf{R}(\alpha)$ is the operator of transformation of the Stokes parameters at rotation of the reference plane through the angle α:

$$\mathbf{R}(\alpha) = \begin{pmatrix} 1 & 0 & 0 & 0 \\ 0 & \cos 2\alpha & \sin 2\alpha & 0 \\ 0 & -\sin 2\alpha & \cos 2\alpha & 0 \\ 0 & 0 & 0 & 1 \end{pmatrix}. \tag{2}$$

0235-6880/00/09 794-07 $02.00

In this work we restrict our consideration to the models of ensembles of hexagonal ice plates and columns, for which the following conditions hold:

– axes of the plates are mostly oriented normally to the horizontal plane (plane xOy, see Fig. 1),

– axes of columns mostly lie in the horizontal plane.

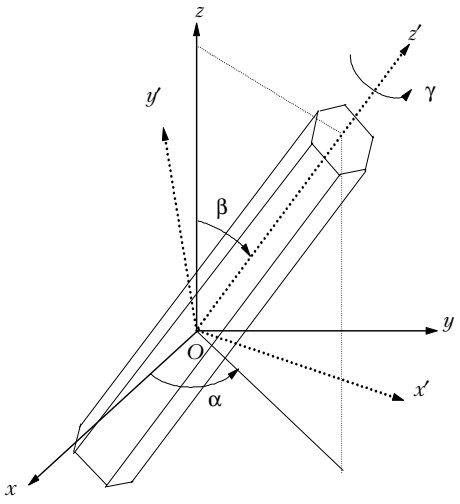

Fig. 1. Geometry of scattering by an arbitrarily oriented hexagonal crystal.

Since in the case of an arbitrarily oriented crystal for the BSPM averaged over the angle γ the following conditions are met: $\mathbf{M}(a, L, \alpha, \beta) = \mathbf{M}(a, L, \alpha + \pi, \beta)$, $\mathbf{M}(a, L, \alpha, \beta) = \mathbf{M}(a, L, \alpha, \pi - \beta)$, then in Eq. (1) it is sufficient to integrate over the angle α from 0 to π and over the angle β from 0 to $\pi/2$. Consequently, Eq. (1) takes the form

$$\mathbf{P}(a, L) = \frac{1}{\pi} \int_0^{\pi} \int_0^{\pi/2} \mathbf{M}(a, L, \alpha, \beta)\, g(\alpha, \beta) \sin\beta \, d\beta \, d\alpha. \quad (3)$$

In the general case, the matrix $\mathbf{M}(a, L, 0, \beta)$ has eight non-zero elements, five of which are linearly independent, and

$$M_{11}(a, L, 0, \beta) - M_{22}(a, L, 0, \beta) + M_{33}(a, L, 0, \beta) - M_{44}(a, L, 0, \beta) = 0,$$

$$M_{21}(a, L, 0, \beta) = M_{12}(a, L, 0, \beta),$$

$$M_{43}(a, L, 0, \beta) = -M_{34}(a, L, 0, \beta).$$

For brevity, let us present $\mathbf{M}(a, L, 0, \beta)$ in the following form:

$$\mathbf{M}(a, L, 0, \beta) = \begin{pmatrix} M_{11} & M_{12} & 0 & 0 \\ M_{12} & M_{22} & 0 & 0 \\ 0 & 0 & M_{33} & M_{34} \\ 0 & 0 & -M_{34} & M_{44} \end{pmatrix}, \quad (4)$$

where all elements of the matrix depend on a, L, and β.

Assume that crystal axes have some dominant orientation relative to the lidar-related coordinate system $Oxyz$ (see Fig. 1). The probability density of orientation of the crystal axes for such an ensemble can be written in the form of the product of two probability densities of orientation with respect to the azimuthal and polar angles:

$$g^{p,c}(\alpha, \alpha_m, k_\alpha, \beta, k_\beta) = f(\alpha, \alpha_m, k_\alpha)\, h^{p,c}(\beta, k_\beta), \quad (5)$$

where

$$f(\alpha, \alpha_m, k_\alpha) = \exp[k_\alpha \cos 2(\alpha - \alpha_m)] / I_0(k_\alpha)$$

is the probability density of the crystal axis orientation with respect to the azimuthal angle α [the distribution similar to the Mises distribution,[8] but differing by the presence of factor 2 in the cosine argument in Eq. (5)]; $I_0(k_\alpha)$ is the modified first-kind zero-order Bessel function; α_m is the modal angle of the distribution; k_α is the parameter characterizing the degree of orientation of crystals with respect to the modal value of the angle; $h^{p,c}(\beta, k_\beta)$ is the probability density of orientation of crystal axes with respect to the polar angle β for plates and columns (superscripts p and c, respectively), k_β is the parameter characterizing the degree of orientation of crystals with respect to the horizontal plane.

Note that for the function $f(\alpha, \alpha_m, k_\alpha)$ the following conditions are met:

$$\int_0^{\pi} f(\alpha, \alpha_m, k_\alpha)\, d\alpha = \pi;$$

$$f(\alpha, \alpha_m, 0) = 1, \quad f(\alpha, \alpha_m, k_\alpha) = f(\alpha + \pi, \alpha_m, k_\alpha).$$

Since we failed to find in the literature the functions $h^{p,c}(\beta, k_\beta)$ convenient for calculation, we propose to determine them based on the following conditions:

1) $\int_0^{\pi/2} h^{p,c}(\beta, k_\beta) \sin(\beta)\, d\beta = 1;$

2) $h^{p,c}(\beta, k_\beta) = h^{p,c}(\pi - \beta, k_\beta);$

3) Since plate axes are mostly oriented normally to the horizontal plane, the function $h^p(\beta, k_\beta)$ achieves its maximum at $\beta = 0$ and $\beta = \pi$;

4) Since column axes mostly lie in the horizontal plane, the function $h^c(\beta, k_\beta)$ achieves the maximum at $\beta = \pi/2$;

5) $\lim_{k_\beta \to 0} h^c(\beta, k_\beta) = \lim_{k_\beta \to 0} h^p(\beta, k_\beta) = 1.$

Thus, the probability density of orientation of crystal axes in space at $k_\alpha = k_\beta = 0$ describes chaotic orientation of crystals, i.e., the function $g^{p,c}(\alpha, \alpha_m, 0, \beta, 0)$ is equal to unity.

Based on the conditions listed above, we have constructed the functions of the probability density of

orientation of axes of hexagonal plates and columns with respect to the polar angle β in the following form:

$$h^{\mathrm{p}}(\beta, k_\beta) = k_\beta \exp[k_\beta |\cos\beta|]/[\exp(k_\beta) - 1],$$

$$h^{\mathrm{c}}(\beta, k_\beta) = k_\beta \exp[-k_\beta |\cos\beta| - 1]/[\exp(k_\beta) - 1].$$

Figure 2 exemplifies the probability densities of crystal axis orientation $f(\alpha, \pi/2, k_\alpha)$, $h^{\mathrm{p}}(\beta, k_\beta)$, and $h^{\mathrm{c}}(\beta, k_\beta)$ for different values of the parameters k_α and k_β.

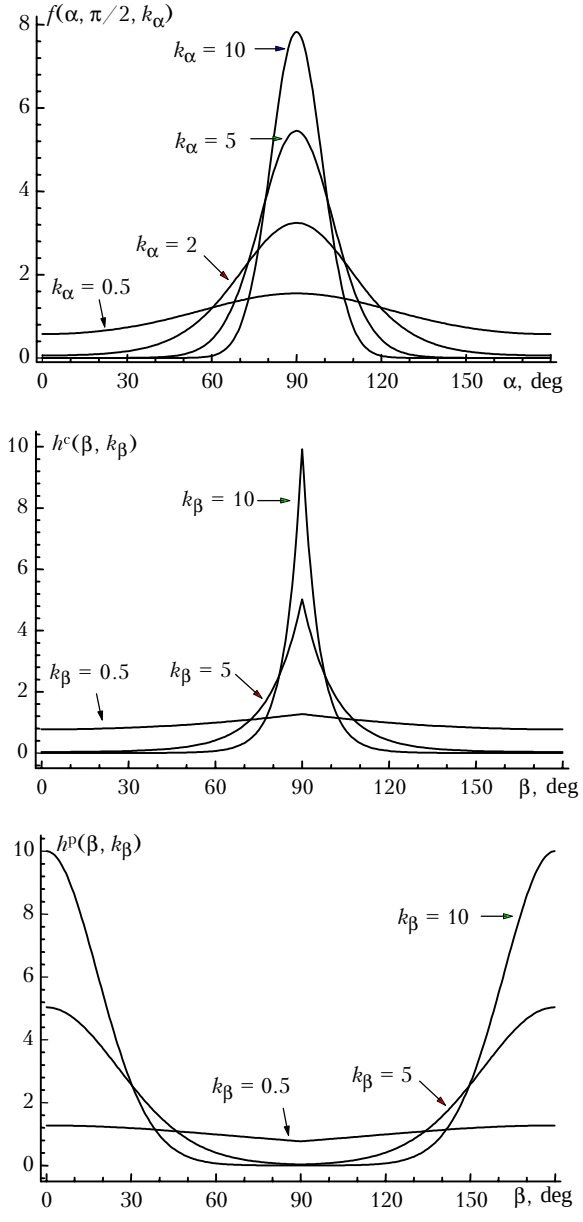

Fig. 2. Functions of probability density of orientation of plate and column axes with respect to the polar angle β [$h^{\mathrm{p}}(\beta, k_\beta)$ and $h^{\mathrm{c}}(\beta, k_\beta)$] and azimuthal angle α [$f(\alpha, \pi/2, k_\alpha)$] at different values of the orientation parameters k_β and k_α.

Upon integration of Eq. (3) over the angles β and α using Eqs. (2), (4), and (5), we obtain

$$\mathbf{P}(a, L, \alpha_{\mathrm{m}}, \beta_{\mathrm{m}}) =$$

$$= \begin{pmatrix} G_{11} & i_1 G_{12}\cos 2\alpha_m & -i_1 G_{12}\sin 2\alpha_{\mathrm{m}} & 0 \\ i_1 G_{12}\cos 2\alpha_{\mathrm{m}} & U + i_2 W\cos 4\alpha_{\mathrm{m}} & -i_2 W\sin 4\alpha_{\mathrm{m}} & -i_1 G_{34}\sin 2\alpha_{\mathrm{m}} \\ i_1 G_{12}\sin 2\alpha_{\mathrm{m}} & i_2 W\sin 4\alpha_{\mathrm{m}} & -U + i_2 W\cos 4\alpha_{\mathrm{m}} & i_1 G_{34}\cos 2\alpha_{\mathrm{m}} \\ 0 & -i_1 G_{34}\sin 2\alpha_{\mathrm{m}} & -i_1 G_{34}\cos 2\alpha_{\mathrm{m}} & G_{44} \end{pmatrix} \quad (6)$$

where $i_1(k_\alpha) = I_1(k_\alpha)/I_0(k_\alpha)$, $i_2(k_\alpha) = I_2(k_\alpha)/I_0(k_\alpha)$, I_0, I_1, I_2 are the modified first-kind Bessel functions of the zero, first, and second orders, respectively;

$$U = (G_{22} - G_{33})/2; \quad W = (G_{22} + G_{33})/2;$$

$$G_{ij}^{\mathrm{p,c}}(a, L, k_\beta) = \int_0^{\pi/2} M_{ij}(a, L, 0, \beta) \times$$

$$\times h^{\mathrm{p,c}}(\beta, k_\beta) \sin(\beta)\, \mathrm{d}\beta, \quad i, j = 1, 2, 3, 4. \quad (7)$$

Thus, to obtain the BSPM of an ensemble of monodisperse poly-oriented hexagonal crystals, it is sufficient to calculate the matrix $\mathbf{M}(a, L, 0, \beta)$ in the form of a table with a rather small step in the angle β (especially, near the points $\beta = 0$ and $\beta = \pi/2$). Elements of this matrix for different values of the parameters a, L, and β are the least basic elements of the data bank for interpreting the results of laser polarization sensing of crystalline clouds.

Figure 3 shows the k_β dependence of the four reduced elements of the scattering matrix **G** for three different monodisperse ensembles of ice hexagonal plates, whose axes lie in the reference plane. The plate axes are assumed to be mostly oriented vertically. The corresponding dependence of the same integral elements for three different monodisperse ensembles of ice hexagonal columns is shown in Fig. 4.

From the behavior of the curves shown in Figs. 3 and 4 we can draw the following conclusions:

– with the growth of k_β, the values of all elements of **G** asymptotically tend to the values of the analogous elements of the BSPM for spherical particles;

– the values of G_{22}/G_{11} for plates are much smaller than those for columns;

– the values of G_{44}/G_{11} for plates are much greater than those for columns;

– the values of G_{34}/G_{11} for columns are larger than those for plates;

– the values of G_{12}/G_{11} at small values of k_β decrease with increasing size of a crystal.

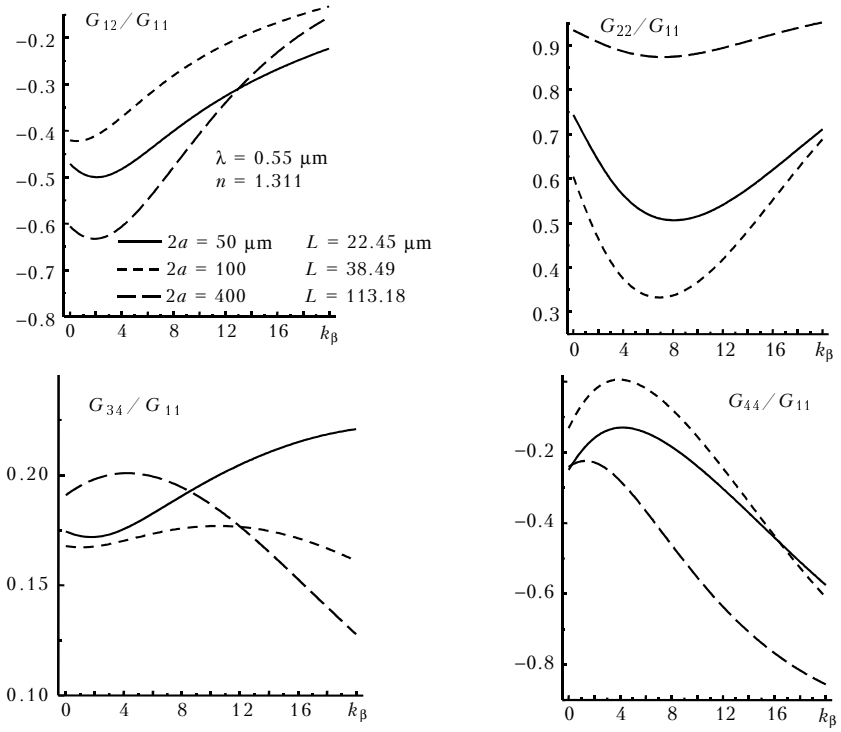

Fig. 3. Dependence of elements of the backscattering phase matrix **G** for monodisperse ensembles of different-size hexagonal ice plates whose axes lie in the reference plane on k_β [k_β is the degree of orientation of their axes with respect to the modal angle $\beta_m = 0$ (plate flatter)].

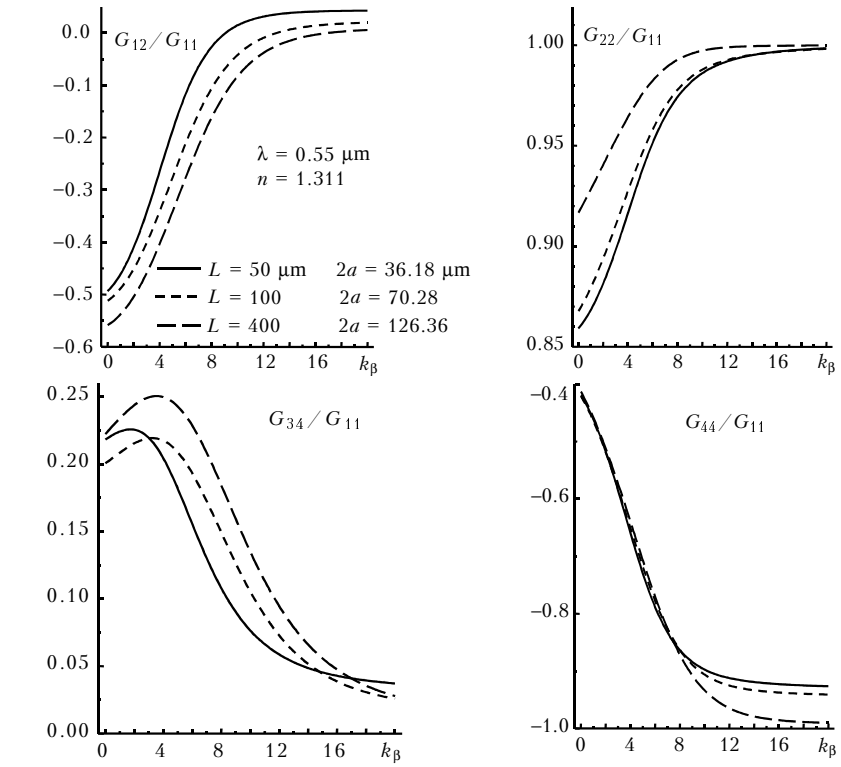

Fig. 4. Dependence of elements of the backscattering phase matrix **G** for monodisperse ensembles of different-size hexagonal ice columns whose axes lie in the reference plane on k_β [k_β is the degree of orientation of their axes with respect to the modal angle $\beta_m = \pi/2$ (column flatter)].

2. Data bank for interpreting results of laser polarization sensing of crystalline clouds

At the time we wrote this paper, the data bank contained 2D data arrays on $\mathbf{M}(a_j, L_j, 0, \beta_i)$, $j = 1, 2, \ldots, 110$; $i = 0, 1, 2, \ldots, 466$, for five types of hexagonal ice crystals. All values of $\mathbf{M}(a_j, L_j, 0, \beta_i)$ were computed using the program developed based on the beam splitting method[3,9] for the incident radiation wavelength $\lambda = 0.55$ μm and the refractive index $n = 1.311$.

The arrays of $\mathbf{M}(a_j, L_j, 0, \beta_i)$ values are two-dimensional, because the relation between a_j and L_j was set functionally in the form

$$L_j = A(2\ a_j)^{\rho},$$

where A and ρ are constants, whose values for the five above-listed types of hexagonal ice crystals are borrowed from Ref. 10 and given in Table 1.

Table 1. Empirical relations between $2a$ and L for hexagonal ice crystals whose BSPM's are contained in the data bank

Type of crystals	A	ρ	Length of the longest axis, μm
Thin plates	1.79	0.474	from 10 to 3000
Thick plates	1.07	0.778	from 10 to 1000
Long columns	$1.48 \cdot 10^{-2}$	2.288	from 50 to 4000
Columns $L/2a > 2$	2.07	1.079	from 10 to 1000
Columns $L/2a < 2$	1.18	1.044	from 10 to 1000

Note that the dimension of the array β_i is fixed, whereas the dimension of the arrays a_j and L_j is variable, i.e., the data bank can be continuously complemented with data for crystals of various size and type.

3. Interpretation of measured BSPM's

The experimental backscattering matrix **S** was interpreted by the MODFIND program with the use of the data bank. The input parameters for this program are: the experimentally measured BSPM $\mathbf{S}(4\times4)$, the modal value β_m of the angle β, the maximum value $k_{\beta max}$ of the parameter k_β, and the maximum acceptable absolute value of the difference between the elements S_{44}/S_{11} of the experimental BSPM and P_{44}/P_{11} of the model BSPM (thd). The values of the model BSPM are set in the text file bsm.ind. The resulting parameters that are outputted into the text file bsm.out are a, L, α_m, k_α, β_m, k_β, and **P**.

At the first stage, the MODFIND program reads the cross section of the $\mathbf{M}(a_j, L_j, 0, *)$ array sequentially for every fixed j for all angles β_i, $i = 0, 1, \ldots, 466$. For every fixed section, the program models by Eq. (7) the matrices $\mathbf{G}(a_j, L_j, k_\beta)$ for the values of k_β from 0 to $k_{\beta max}$ with the step $\Delta k_\beta = 0.1$. The matrices **G** not satisfying the condition $|G_{44}/G_{11} - S_{44}/S_{11}| \le$ thd are omitted from further consideration. The angle of the dominant orientation α_m is determined with the help of the equalities $\mathbf{S} \approx \mathbf{P}$ and Eq. (6). Then, for every fixed matrix **G**, the program models different matrices **P** by Eq. (6). The matrices **P**, for whose elements the conditions $|P_{22}/P_{11} - S_{22}/S_{11}| \le$ thd, $|P_{33}/P_{11} - S_{33}/S_{11}| \le$ thd, $|P_{12}/P_{11} - S_{12}/S_{11}| \le$ thd are satisfied, are outputted together with the parameters a, L, α_m, k_α, β_m, and k_β in the output text file.

To illustrate how the MODFIND program operates with the data from the data bank, we have interpreted three measured BSPMs having different structure. Table 2 presents the interpretation of the measured matrix from Ref. 11. This BSPM is characterized by very high absolute values of S_{12}/S_{11} and S_{34}/S_{11}. As a result, the model ensemble of hexagonal ice columns, whose calculated BSPM is the closest to the measured one, has high values of k_α and low values of k_β. Thus, the column axes are only slightly oriented with respect to the horizontal plane and highly oriented with respect to the lidar basis plane. This orientation is likely connected with very high eastern jet flows (the lidar basis plane roughly coincided with the meridional plane during measurements).

Table 3 presents the model ensembles of plate ice crystals, whose BSPM **P** is the closest to the measured one **S** (Ref. 2). The values of microstructure parameters show that the ensembles consist of both fine and coarse plates, whose axes are oriented almost vertically with a small flatter, and the pronounced orientation with respect to the reference plane is absent.

The third measured matrix **S** was calculated by averaging the altitude profiles of BSPM from Ref. 11 at the altitudes from 7.5 to 8.5 km. It turns out that the chosen layer can be very well interpreted by model ensembles of large thick ice plates from 400 to 1000 μm in diameter. The results of interpretation of the measured BSPM are presented in Table 4. The values of the parameters k_α and k_β in Table 4 show that the plate axes have pronounced vertical orientation with a rather large flatter, and they are not strictly oriented with respect to the lidar basis plane.

The analysis of the behavior of the parameters k_α and k_β in Tables 2–4 for the same crystal allows the conclusion that the more oriented are crystals (plates with axes directed vertically, and columns with axes directed horizontally), the more oriented they are with respect to the reference plane.

In Ref. 2, the experimentally measured BSPM's (see Tables 2 and 4) were compared with the matrices calculated based on the model of cylindrical backscattering matrices. The analysis of the both model calculated BSPM's shows that model ensembles of hexagonal ice crystals provide much more close description of the regularities of backscattering in crystalline clouds.

Table 2. Results of comparison of the calculated matrices P and experimentally measured BSPM (bottom row)

α_m	k_α	k_β	a, μm	L, μm	P_{22}	P_{33}	P_{44}	P_{12}	P_{13}	P_{34}	P_{24}	P_{23}
90.00	3.96	0.50	13.07	70.00	0.779	−0.553	−0.332	0.431	0.000	−0.186	0.000	0.000
90.00	3.76	0.50	16.49	90.00	0.783	−0.563	−0.347	0.435	0.000	−0.181	0.000	0.000
90.00	3.60	0.50	22.36	125.00	0.785	−0.569	−0.354	0.438	0.000	−0.184	0.000	0.000
90.00	3.46	0.50	26.48	150.00	0.781	−0.566	−0.347	0.439	0.000	−0.186	0.000	0.000
90.00	3.36	0.50	34.57	200.00	0.782	−0.569	−0.351	0.441	0.000	−0.186	0.000	0.000
90.00	3.22	0.50	50.34	300.00	0.776	−0.565	−0.342	0.444	0.000	−0.205	0.000	0.000
90.00	3.04	0.50	124.93	800.00	0.785	−0.560	−0.345	0.431	0.000	−0.206	0.000	0.000
90.00	4.08	0.60	13.07	70.00	0.783	−0.554	−0.337	0.430	0.000	−0.188	0.000	0.000
90.00	3.68	0.60	14.79	80.00	0.775	−0.557	−0.332	0.437	0.000	−0.186	0.000	0.000
90.00	3.86	0.60	16.49	90.00	0.787	−0.566	−0.353	0.434	0.000	−0.183	0.000	0.000
90.00	3.54	0.60	26.48	150.00	0.785	−0.568	−0.354	0.439	0.000	−0.187	0.000	0.000
90.00	3.28	0.60	50.34	300.00	0.779	−0.568	−0.348	0.444	0.000	−0.206	0.000	0.000
90.00	3.10	0.60	124.93	800.00	0.789	−0.563	−0.352	0.431	0.000	−0.207	0.000	0.000
90.00	4.20	0.70	13.07	70.00	0.786	−0.556	−0.343	0.429	0.000	−0.189	0.000	0.000
90.00	3.76	0.70	14.79	80.00	0.778	−0.559	−0.337	0.436	0.000	−0.188	0.000	0.000
90.00	3.98	0.70	16.49	90.00	0.791	−0.568	−0.359	0.433	0.000	−0.184	0.000	0.000
90.00	3.16	0.70	124.93	800.00	0.794	−0.566	−0.360	0.430	0.000	−0.209	0.000	0.000
90.00	4.36	0.80	13.07	70.00	0.790	−0.557	−0.348	0.427	0.000	−0.191	0.000	0.000
90.00	3.84	0.80	14.79	80.00	0.781	−0.561	−0.342	0.435	0.000	−0.189	0.000	0.000
90.00	3.22	0.80	124.93	800.00	0.798	−0.569	−0.367	0.429	0.000	−0.210	0.000	0.000
90.00	4.56	0.90	13.07	70.00	0.795	−0.558	−0.354	0.426	0.000	−0.193	0.000	0.000
90.00	3.94	0.90	14.79	80.00	0.784	−0.563	−0.347	0.434	0.000	−0.190	0.000	0.000
90.00	4.78	1.00	13.07	70.00	0.799	−0.560	−0.359	0.425	0.000	−0.195	0.000	0.000
90.00	4.06	1.00	14.79	80.00	0.788	−0.564	−0.353	0.433	0.000	−0.192	0.000	0.000
90.00	4.18	1.10	14.79	80.00	0.792	−0.566	−0.358	0.432	0.000	−0.194	0.000	0.000
90.00	4.32	1.20	14.79	80.00	0.796	−0.568	−0.364	0.430	0.000	−0.195	0.000	0.000
Experiment (Ref. 11) thd = 0.025					S_{22}	S_{33}	S_{44}	S_{12}	S_{13}	S_{34}	S_{24}	S_{23}
					0.780	−0.550	−0.350	0.430	0.000	−0.280	0.000	0.000

Table 3. Results of comparison of the calculated matrices P and experimentally measured BSPM (bottom row)

α_m	k_α	k_β	a, μm	L, μm	P_{22}	P_{33}	P_{44}	P_{12}	P_{13}	P_{34}	P_{24}	P_{23}
86.20	0.50	4.00	500.00	230.88	0.671	−0.655	−0.326	0.148	0.019	−0.050	−0.006	−0.002
86.20	0.50	4.10	500.00	230.88	0.674	−0.657	−0.331	0.147	0.019	−0.050	−0.006	−0.002
86.20	0.60	4.50	150.00	90.49	0.672	−0.655	−0.327	0.147	0.019	−0.056	−0.007	−0.002
86.20	0.60	4.60	150.00	90.49	0.674	−0.657	−0.332	0.147	0.019	−0.056	−0.007	−0.002
86.20	0.54	5.20	200.00	113.18	0.671	−0.657	−0.329	0.148	0.019	−0.051	−0.006	−0.001
86.20	0.54	5.30	200.00	113.18	0.673	−0.659	−0.333	0.147	0.019	−0.051	−0.006	−0.001
86.20	0.54	5.70	300.00	155.16	0.669	−0.658	−0.327	0.146	0.019	−0.050	−0.006	−0.001
86.20	0.54	5.80	300.00	155.16	0.671	−0.660	−0.331	0.145	0.019	−0.050	−0.006	−0.001
86.20	0.56	5.90	300.00	155.16	0.673	−0.662	−0.335	0.149	0.019	−0.052	−0.006	−0.001
86.20	0.66	6.40	15.00	15.09	0.665	−0.659	−0.325	0.148	0.019	−0.062	−0.008	−0.000
86.20	0.66	6.50	15.00	15.09	0.666	−0.661	−0.327	0.148	0.019	−0.062	−0.008	−0.000
86.20	0.66	6.60	15.00	15.09	0.667	−0.662	−0.330	0.147	0.019	−0.062	−0.008	−0.000
86.20	0.66	6.70	15.00	15.09	0.668	−0.663	−0.332	0.146	0.019	−0.062	−0.008	−0.000
86.20	0.66	6.80	15.00	15.09	0.670	−0.665	−0.335	0.146	0.019	−0.063	−0.008	−0.000
86.20	0.68	6.90	15.00	15.09	0.671	−0.666	−0.338	0.149	0.019	−0.064	−0.008	−0.000
86.20	0.68	7.00	15.00	15.09	0.672	−0.668	−0.340	0.148	0.019	−0.065	−0.008	−0.000
86.20	0.68	7.10	15.00	15.09	0.674	−0.669	−0.343	0.148	0.019	−0.065	−0.008	−0.000
86.20	1.16	9.30	100.00	66.01	0.659	−0.669	−0.329	0.148	0.019	−0.093	−0.012	0.001
86.20	1.18	9.40	100.00	66.01	0.661	−0.672	−0.334	0.149	0.019	−0.094	−0.012	0.001
Experiment (Ref. 2) thd = 0.025					S_{22}	S_{33}	S_{44}	S_{12}	S_{13}	S_{34}	S_{24}	S_{23}
					0.650	−0.650	−0.350	0.150	0.020	−0.100	−0.005	0.000

Table 4. Results of comparison of the calculated matrices P and experimentally measured BSPM (bottom row)

α_m	k_α	k_β	a, μm	L, μm	P_{22}	P_{33}	P_{44}	P_{12}	P_{13}	P_{34}	P_{24}	P_{23}
88.84	1.36	3.60	450.00	212.71	0.714	−0.612	−0.327	0.349	0.014	−0.115	−0.004	−0.004
88.84	1.34	3.70	400.00	194.08	0.714	−0.611	−0.325	0.350	0.014	−0.110	−0.004	−0.004
88.84	1.38	3.70	450.00	212.71	0.718	−0.614	−0.332	0.350	0.014	−0.117	−0.004	−0.004
88.84	1.36	3.80	400.00	194.08	0.717	−0.613	−0.330	0.352	0.014	−0.112	−0.004	−0.004
88.84	1.40	3.80	450.00	212.71	0.721	−0.616	−0.338	0.351	0.014	−0.118	−0.004	−0.004
88.84	1.36	3.90	400.00	194.08	0.719	−0.616	−0.336	0.350	0.014	−0.112	−0.004	−0.004
88.84	1.42	4.00	350.00	174.93	0.715	−0.613	−0.328	0.354	0.014	−0.111	−0.004	−0.004
88.84	1.38	4.00	400.00	194.08	0.722	−0.618	−0.341	0.352	0.014	−0.113	−0.004	−0.004
88.84	1.40	4.00	500.00	230.88	0.715	−0.610	−0.326	0.352	0.014	−0.120	−0.004	−0.004
88.84	1.44	4.10	350.00	174.93	0.718	−0.615	−0.333	0.355	0.014	−0.112	−0.004	−0.004
88.84	1.40	4.10	500.00	230.88	0.717	−0.614	−0.331	0.350	0.014	−0.120	−0.004	−0.004
88.84	1.44	4.20	350.00	174.93	0.720	−0.618	−0.339	0.353	0.014	−0.112	−0.004	−0.004
88.84	1.42	4.20	500.00	230.88	0.721	−0.616	−0.337	0.351	0.014	−0.122	−0.004	−0.004
88.84	1.46	4.30	350.00	174.93	0.723	−0.621	−0.344	0.354	0.014	−0.113	−0.004	−0.004
88.84	1.42	4.30	500.00	230.88	0.723	−0.619	−0.342	0.349	0.014	−0.122	−0.004	−0.004
88.84	1.76	5.10	250.00	134.64	0.705	−0.620	−0.326	0.388	0.015	−0.120	−0.004	−0.003
88.84	1.64	5.20	200.00	113.18	0.714	−0.614	−0.329	0.360	0.014	−0.125	−0.005	−0.004
88.84	1.66	5.30	200.00	113.18	0.716	−0.616	−0.333	0.361	0.014	−0.126	−0.005	−0.004
88.84	1.66	5.40	200.00	113.18	0.718	−0.619	−0.337	0.359	0.014	−0.126	−0.005	−0.004
88.84	1.68	5.50	200.00	113.18	0.720	−0.621	−0.342	0.359	0.014	−0.127	−0.005	−0.004
Experiment (Ref. 11) thd = 0.025					S_{22}	S_{33}	S_{44}	S_{12}	S_{13}	S_{34}	S_{24}	S_{23}
					0.704	−0.602	−0.345	0.359	0.015	−0.090	−0.054	−0.009

Acknowledgments

This work was partially supported by the Russian Foundation for Basic Research (Grant No. R98–02–03031) and the Ministry of Science of the Russian Federation (Project No. 06–21).

References

1. D.N. Romashov and R.F. Rakhimov, Atmos. Oceanic Opt. **6**, No. 8, 515–518 (1993).
2. B.V. Kaul', D.N. Romashov, and I.V. Samokhvalov, Atmos. Oceanic Opt. **10**, No. 10, 697–701 (1997).
3. D.N. Romashov, Atmos. Oceanic Opt. **12**, No. 5, 376–384 (1999).
4. Sun Yi-Yi, Li Zhi-Ping, and J. Boesenberg, Appl. Opt. **28**, No. 17, 3625–3638 (1989).
5. M. Mishchenko and K. Sassen, Geophys. Res. Lett. **25**, No. 3, 309–312 (1998).
6. A. Ben-David, J. Geophys. Res. **103**, No. 3, 26.041–26.050 (1998).
7. B.V. Kaul' and D.N. Romashov, Atmos. Oceanic Opt. **10**, No. 12, 931–936 (1997).
8. K. Mardia, *Statistical Analysis of Angle Observations* (Nauka, Moscow, 1978), 239 pp.
9. A.A. Popov, "*Scattering of electromagnetic plane wave on semitransparent convex polyhedron of an arbitrary shape*," Izv. Vyssh. Uchebn. Zaved., Ser. Fizika (Tomsk, 1984), 56 pp., Dep. VINITI, No. 8006.
10. O.P. Volkovitskii, L.P. Pavlov, and A.G. Petrushin, *Optical Properties of Crystalline Clouds* (Gidrometeoizdat, Leningrad, 1984), 200 pp.
11. B.V. Kaul', O.A. Krasnov, A.L. Kuznetsov, E.R. Polovtseva, I.V. Samokhvalov, and A.P. Stykon, Atmos. Oceanic Opt. **10**, No. 2, 119–125 (1997).